Manuscript Click here to view linked References

Chemical Engineering Journal, Volume 512, May 2025, Article number 162796
DOI: 10.1016/j.cej.2025.162796

Machine learning-driven sensor array based on luminescent metal-organic frameworks for simultaneous identification of multiple anions in environmental waters

Dali Wei[1], Yudi Yang[1], Ying Wang[1], Yunxiang Fan[1], Yuxuan Shen[1], Chunmeng Deng[1], Kun Zeng[1], Zhugen Yang[2], Zhen Zhang[1]*

[1]School of the Environment and Safety Engineering, School of the Emergency Management, Jiangsu University, Zhenjiang 212013, China.

[2]School of Water, Energy, and Environment, Cranfield University, Milton Keynes, MK43 0AL, UK.

*Corresponding author:
Email: zhenzhang@ujs.edu.cn.

Published by Elsevier. This is the Author Accepted Manuscript issued with: Creative Commons Attribution License (CC:BY 4.0).
The final published version (version of record) is available online at DOI:10.1016/j.cej.2025.162796. Please refer to any applicable publisher terms of use.

Abstract

Due to the high correlation of anions in waters to environmental quality and human health, thus there is urgent need for developing simple and effective sensors to discriminate multiple anions. Herein, a machine learning-assisted fluorescent sensor array based on two luminescent metal-organic frameworks (LMOFs, UiO-66-NH_2 and UiO-66-OH) was developed for simultaneous discrimination of five anions (F^-, PO_4^{3-}, ClO_4^{4-}, NO_3^-, and SO_4^{2-}). Wherein, UiO-66-NH_2 and UiO-66-OH were designed by anchoring 2,5-diaminoterephthalic acid and 2,5-dihydroxyterephthalic acid on UiO-66, respectively, which exhibited blue and green fluorescence emission, possessing good fluorescence property. Interestingly, the anions could effectively enhance the fluorescence intensity of UiO-66-NH_2 and UiO-66-OH to generate diverse fluorescence responses and unique fingerprints, which could be utilized to develop a fluorescence sensor array for the sensitive identification of five anions and their mixtures. Under the optimized conditions, the limit of detection (LOD) of the proposed array for anions detection was about at 2.14-3.51 μM with a satisfactory accuracy. More importantly, the integration of machine learning algorithm and sensor array has successfully achieved accurate identification and prediction of five anions in real water samples, affirming its practicability in actual samples. Our findings provided a promising tool for detecting multiple anions, and inspired potentials of the combination of sensor arrays and machine learning algorithm for pollution control in real waters.

Keywords: anions detection, sensor array, metal-organic frameworks, environmental monitoring

1. Introduction

Anions play an irreplaceable role in the ecological system, while excessive anions can pose a huge threat to environment quality and human health (Al-Saidi and Khan 2022; Goshisht and Tripathi 2021). For instance, chronic exposure of fluoride (F^-) with high levels can lead to acute gastric and kidney problems or even skeletal fluorosis, and the high concentration of phosphate (PO_4^{3-}) can induce the detrimental effects on aquatic ecosystems, leading to serious human diseases such as hyperparathyroidism (Lin et al. 2019; Yi and Zhang 2020). In addition, excessive nitrate (NO_3^-) can induce eutrophication in waters, while perchlorate (ClO_4^{4-}) with high toxicity also poses threats to human health (Amali et al. 2021; Cao et al. 2019; Liu et al. 2022). To date, various well-established instrumental techniques for anions detection have been reported (Kodamatani et al. 2023; Liu et al. 2023; Norton et al. 2021; Wu et al. 2020; Zhou et al. 2014), whereas these methods were hampered for wide applications by sophisticated equipment, time-consuming detection, and tedious procedures for pretreatment (Amali et al. 2021; Fang and Naidu 2023; Guo et al. 2017; Moumen et al. 2022; Wang et al. 2017). Besides, novel methods based on the specific probes can only accomplish the rapid detection of one or two anions (Zhang et al. 2020). Therefore, it is desirable to develop efficient methods for the identification of multiple anions.

Recently, great efforts have been devoted to explore sensor arrays as an artificial tongue (Wei et al. 2024; Xu et al. 2024), which mimic the mammalian tasting system for the identification of contaminants (Ihde et al. 2022; Meng et al. 2023; Wu et al. 2023), proteins (Lu et al. 2022; Wang et al. 2018), and pathogens (Yu et al. 2023; Zhou et al. 2019), etc. Wherein, fluorescent sensor arrays have attracted wide attentions in the sensing field due to rapid detection, high sensitivity, and capability of multitarget detection, whereas traditional fluorescent sensor arrays often rely on multiple independent sensing elements, which requires higher cost, complicated synthesis, and time-consuming (Nawaz et al. 2020; Sharifi et al. 2021; Zhang et al. 2020). In addition, the application of fluorescent sensor arrays for real samples was still limited. To simply the composition of a sensor array, a basic probe modified with different functional groups as the sensing elements could be an effective strategy to construct sensor arrays, which exhibited the following advantages: (i) sensing units prepared by a basic material

functionalized with various ligands is relatively simple, which requires the similar synthesis method, circumventing the tedious synthesis process; (ii) functional groups were used to bind with various targets, which enabled them to be excellent cross-reactive probes for constructing sensor array. Meanwhile, machine learning, as a powerful data processing tool, presented remarkable capabilities in clustering, regression, and prediction analysis, which could enhance the performance of sensor arrays in actual samples (Jing et al. 2024; Li et al. 2024; Song et al. 2024). Thus, we speculated that machine learning-supported sensor array based on a basic material functionalized with various ligands could realize the low-cost, rapid, and efficient screening, showing the great potentials for the intelligent recognition of multiple anions in environments.

In this study, we prepared two luminescent metal-organic frameworks (LMOFs, UiO-66-NH_2 and UiO-66-OH) by using UiO-66 as basic material functionalized with different ligands to construct a fluorescence sensor array assisted by machine learning for the screening of five anions (**Scheme 1**). Wherein, the fluorescence intensity of two LMOFs enhanced upon the addition of anions owing to the diverse interactions between anions and LMOFs, resulting in unique fluorescence patterns. And five anions and their mixtures were successfully discriminated by the constructed sensor array through the pattern recognition methods. More importantly, powered by machine learning, the proposed sensor array showed good performance in identifying anions in real environmental waters.

2. Materials and methods

2.1 Preparation of UiO-66-NH_2 and UiO-66-OH

UiO-66-NH_2 were synthesized according to the reported literature (Sun et al. 2016; Sun et al. 2020). Typically, $ZrCl_4$ (30 mg, 0.129 mmol) and BDC-$(NH_2)_2$ (20 mg, 0.110 mmol) were dissolved in 2 mL of DMF, and then benzoic acid (600 mg, 4.918 mmol) was added into the above solution and sufficiently dissolved. The above mixture was transferred into hydrothermal reactor and heated to 120 °C for 12 h. Following, the precipitates were collected by centrifugation, and then washed with DMF and acetone for three times, respectively. UiO-66-NH_2 was obtained by drying at 80 °C.

The preparation of UiO-66-OH was relied on the previous study with minor modification (Wang et al. 2021). $ZrCl_4$ (69.91 mg, 0.3 mmol) and BDC-$(OH)_2$ (59.4 mg, 0.3 mmol) were dissolved in the mixed solution containing DMF (21 mL) and acetic acid (7 mL) under vigorous stirring for 15 min. Then, the above solution was heated to 120 ℃ in oil bath under gentle stirring for 8 h, and white precipitates were collected by centrifugation. Following, the precipitates were collected by centrifugation, and then washed with DMF and acetone for three times, respectively. UiO-66-OH was obtained by drying at 80 °C.

2.2 Fabrication of fluorescent sensor array for multiple anions identification

The fluorescent sensor array was comprised of two LMOFs (UiO-66-NH_2 and UiO-66-OH), five anions (F^-, PO_4^{3-}, ClO_4^{4-}, NO_3^-, and SO_4^{2-}), and five replicates. Wherein, 50 μL of UiO-66-NH_2 and UiO-66-OH were separately added into the 5 columns (5 replicates) and 6 rows (blank and 5 anions), and then 50 μL of anion solutions was added into the corresponding rows for incubating 10 min at room temperature. The fluorescence intensities of the mixtures of LMOFs and anions in the wells were recorded with emission wavelength of 450 nm (UiO-66-NH_2) and 536 nm (UiO-66-OH) under an excitation wavelength of 350 nm. Then, the relative fluorescence intensity (F/F_0) was collected, and F and F_0 represented the fluorescence intensities of the two MOFs with and without the presence of anions, respectively. Last. the obtained fluorescence response data (2 LMOFs×5 anions×5 replicates) was processed by LDA and HCA for anions identification. In addition, the identification of different concentrations of individual anions and their mixtures was also accomplished by the proposed fluorescent sensor through the similar method.

2.3 Machine learning-assisted sensor array for anions in actual samples

The application of the proposed sensor array was studied by detecting anions in actual water samples (e.g. river water, tap water, and lake water). Wherein, tap water was collected from our laboratory, meanwhile, and river and lake water samples were obtained from Zhenjiang city in Jiangsu Province. After being filtered, these water samples were spiked into different anions, which were detected by the developed sensor array to assess the potentials of the sensor array in identifying multiple anions in real water samples.

Artificial neural networks (ANN), as one of the representative algorithms of machine learning, are mathematical models that simulate the neural network of the human brain (Ray et

al. 2024), which are further employed to combine with the proposed sensor array for assess the performance in actual water samples. Wherein, we used the MATLAB for the analysis and processing of different anions. Five anions (F^-, PO_4^{3-}, ClO_4^{4-}, NO_3^-, and SO_4^{2-}) and one blank water were tested, each with seven parallel samples and two attribute values (UiO-66-NH_2 and UiO-66-OH), resulting in a total of 84 data points, and original data set were divided into the training set (n=60) and the testing set (n=24), respectively. The ANN algorithm was primarily implemented using the "neural network" module, and a confusion matrix was utilized to verify its effectiveness in distinguishing real samples.

3. Results and discussion

3.1 Characterization of UiO-66-NH_2 and UiO-66-OH

UiO-66-NH_2 and UiO-66-OH with different ligands (BDC-$(NH_2)_2$ and BDC-$(OH)_2$) were obtained by a facile solvothermal method (**Fig. 1a**). Wherein, UiO-66-NH_2 exhibited typical octahedral morphology in TEM images, and the average size was about 250 nm (**Fig. 1b**), which was also evidenced by the SEM images (**Fig. 1c**). The generated UiO-66-NH_2 was further assessed by the element distribution of C, N, O, and Zr on a line scan and mapping images (**Fig. 1d-e**). Meanwhile, the correct preparation of UiO-66-OH was also identified by TEM and SEM. Interestingly, the morphology of UiO-66-OH was determined to be a spherical structure with a size of about 100 nm (**Fig. 1f-g**). In addition, the elements of C, N, O, and Zr were obviously observed in the EDS elemental line scan and corresponding element mapping (**Fig. 1h-i**), which verified the successful preparation of UiO-66-OH. Then, the preparation of the UiO-66-NH_2 and UiO-66-OH were further evaluated by ultraviolet absorption, XRD, FTIR, XPS, and nitrogen adsorption/desorption. Shown in **Fig. 2a**, UiO-66-NH_2 had an absorption peak at 260 nm and a wide absorption in the range of 270-340 nm. Wherein, the absorption of UiO-66-NH_2 near 260 nm was attributed to the absorption overlap between the π-π* electron transition of the organic connector in the benzene ring and the Zr-O cluster in the metal coordination center (Chun-Yi Sun 2013), and the absorption band around 270-340 nm was attributed to the N-π* transition of the lone pair of electrons on the ligand amino group (Huilin Zhu 2019). Meanwhile, UiO-66-OH had two wide characteristic absorption peaks at 230-270 nm and 320-425 nm. In addition, the XRD patterns of the obtained UiO-66-NH_2 displayed

three characteristic peaks of 7.36°, 8.48°, and 25.68° (**Fig. 2b**), which were attributed to the crystal face of (111), (002), and (600), and the sharp peaks also indicated a high degree of crystallinity (Fan et al. 2023). Meanwhile, the similar crystal planes were also observed in XRD patterns of UiO-66-OH (Xin et al. 2022). The FTIR spectra of UiO-66-NH_2 and UiO-66-OH were displayed in **Fig. 2c**. the UiO-66-NH_2 had a wide absorption peak around 3430 cm^{-1}, which was ascribed to N-H stretching vibration of NH_2 groups. The peak observed at 1250 cm^{-1} and 1338 cm^{-1} were attributed to the stretching of the C-N bond between carbon and nitrogen in the aromatic group (Fan et al. 2023). For UiO-66-OH, the peak was at 1240 cm^{-1} was related to C-O stretching of OH functional groups on benzene rings (Rada et al. 2016). In addition, the peaks ranging from 600 to 800 cm^{-1} in UiO-66-NH_2 and UiO-66-OH could be ascribed to the Zr-O functional group, implying the coordination between Zr^{4+} and O atoms in BDC-$(NH_2)_2$ and BDC-$(OH)_2$ (Sun et al. 2020).

In addition, as depicted in **Fig. 2d** and **2g**, the characteristic peaks of O 1s, N 1s, C 1s, and Zr 3d appeared in the XPS spectrum of UiO-66-NH_2 and UiO-66-OH, and the elemental contents of Zr in UiO-66-NH_2 and UiO-66-OH were 6.13% and 16.75% (**Table S1 and S2**), respectively, indicating that the successful preparation of two LMOFs. Interestingly, the N 1s peak of UiO-66-NH_2 was sharper than that of UiO-66-OH, which was attributed to the abundance of -NH_2 groups in UiO-66-NH_2. Wherein, two peaks at 182.98 and 185.38 eV in the Zr 3d spectrum of UiO-66-NH_2 were ascribed to the binding energies for Zr $3d_{5/2}$ and Zr $3d_{3/2}$ (**Fig. 2e**), and similar results were observed in UiO-66-OH (**Fig. 2h**). Meanwhile, as shown in **Fig. 2f and 2i**, the three peaks of C 1s spectrum in UiO-66-NH_2 and UiO-66-OH were classified as C-C, C-O, and O-C=O (Wang and Wang 2022). In addition, the O 1s spectrum of UiO-66-NH_2 was divided into three peaks at 530.3, 531.3, and 532.6 eV (**Fig. S1**), which were accounted for the binding energies of Zr-O-Zr, Zr-OH, and -OH, respectively, demonstrating the coordination between Zr^{4+} and O atoms in BDC-NH_2 (Zhu et al. 2014). Similarly, the O 1s spectrum of UiO-66-NH_2 was given **Fig. S2**, suggesting the combination of Zr^{4+} and O atoms in BDC-$(OH)_2$. Besides, the Brunauer-Emmett-Teller (BET) surface area of UiO-66-NH_2 and UiO-66-OH were 614.1 m^2/g^{-1} and 1364.6 m^2/g^{-1}, respectively, and the UiO-66-NH_2 had smaller pore size (3.89 nm) than that of UiO-66-OH (4.91 nm) (**Fig. S3**). Meanwhile, the UiO-66-NH_2 and UiO-66-OH presented positive (+48.6 mV) and negative

charges (-3.43 mV), respectively (**Fig. S4**). All these results revealed the form of UiO-66-NH_2 and UiO-66-OH.

3.2 Luminescent property of UiO-66-NH_2 and UiO-66-OH

Following, the fluorescence properties of UiO-66-NH_2 and UiO-66-OH was further studied. Seen in **Fig. 2j**, the synthesized UiO-66-NH_2 and UiO-66-OH presented fluorescence emission at 450 nm and 536 nm under an excitation wavelength of 350 nm, respectively. Then, the luminescent property of UiO-66-NH_2 and UiO-66-OH were further evaluated by fluorescence lifetime and stability. As shown in **Fig. 2k and Table S2**, the average fluorescence lifetime of UiO-66-NH_2 and UiO-66-OH were 15.74 ns and 3.24 ns, respectively, indicating the good luminescent property of two LMOFs. To further study the fluorescence stability of UiO-66-NH_2 and UiO-66-OH, two MOFs were assessed in some external environments including UV irradiation, long storage, and different pH. Shown in **Fig. S5**, the synthesized UiO-66-NH_2 and UiO-66-OH could maintain good fluorescence performance after the treatment of UV irradiation and different pH. Meanwhile, after the storage of 30 days, the fluorescence intensities of UiO-66-NH_2 and UiO-66-OH only decreased about 15-20% (**Fig. 2i**), indicating the good fluorescence and stability. Thus, all the above proofs also confirmed the good luminescent performance of UiO-66-NH_2 and UiO-66-OH.

3.3 Fluorescence sensor array for discrimination of anions

UiO-66-NH_2 and UiO-66-OH were unitized to design a fluorescence sensor array for rapid discrimination of five anions, including F^-, PO_4^{3-}, ClO_4^{4-}, NO_3^-, and SO_4^{2-} (**Fig. 3a**). The sensing mechanism of the proposed sensor array was relied on the fluorescence response patterns (F/F_0) of anions to two LMOFs with an excitation wavelength of 350 nm, wherein F and F_0 described the emission intensities of two MOFs at in the presence or absence of anions in the reaction systems, respectively. As shown in **Fig. 3b**, the fluorescence intensities of two LMOFs increased with the addition of anions, and the increase degree varied with the types of LMOFs and anion. Wherein, the enhancement effect of F^- on UiO-66-OH was the most significant (about 3 times), followed by PO_4^{3-}, NO_3^-, SO_4^{2-}, and ClO_4^{4-}. By contrast, the addition of PO_4^{3-} could observably improve the fluorescence response of UiO-66-NH_2, followed by F^-. And radar plot of fluorescence responses also indicated that the proposed sensor array showed a good separation ability for these anions (**Fig. 3c**). In addition, the corresponding

heat map illustrated the different fluorescence response of UiO-66-NH_2 and UiO-66-OH to six anions (**Fig. 3d**). The obtained fluorescence response patterns were processed by linear discriminant analysis (LDA) and hierarchical cluster analysis (HCA). Wherein, the LDA results showed distinct distributions of five anions, with no overlap observed (**Fig. 3e**), revealing that the developed sensor array could be employed for anions identification. Meanwhile, five anions were correctly distributed to their respective groups with no misclassification (**Fig. 3f**). Therefore, the above results suggested that the proposed fluorescence sensor array realized rapid discrimination of anions with high confidence.

3.4 Sensing mechanisms of fluorescence sensor array for anions

To explore the sensing mechanism of the proposed fluorescence sensor array toward anions, we chose UiO-66-NH_2 and F^- as an example to uncover the underlying principles. Despite the introduction of F^- could enhance the fluorescence intensity of UiO-66-NH_2, the fluorescence lifetime of UiO-66-NH_2 could not improve (**Fig. 4a** and **Table S2**). Thus, we speculated that the enhanced fluorescence behavior of UiO-66-NH_2 may be related to the interaction between F^- and UiO-66-NH_2, which rearranged the electron cloud of whole framework (Huilin Zhu 2019; Qiaoyin Li 2023). First, the radius of F^- is about 1.33 Å, which is smaller than the pore sizes of UiO-66- NH_2, thus F^- can access to UiO-66-NH_2 to couple the ligand, and then transfer the absorbed energy to the ligand and sensitize its luminescence (Qiaoyin Li 2023; Yaqiong Zhang 2021). Then, the interactions between F^- and UiO-66-NH_2 was revealed by XRD, TEM, zeta potentials, and XPS studies. As shown in **Fig. 4b**, the combination of F^- and UiO-66-NH_2 had no obvious effects on the morphology of UiO-66-NH_2, but the F element was evenly distributed on UiO-66-NH_2, confirming the interaction of F^- and UiO-66-NH_2 (**Fig. 4c**). Meanwhile, the measured zeta potential changes of UiO-66-NH_2 from +48.6 to +41.8 mV after the addition of F^- (**Fig. 4d**), suggesting the combination of F^- and UiO-66-NH_2 (Huilin Zhu 2019). Then, XPS was also performed to study the interactions between F^- and UiO-66-NH_2. As shown in **Fig. 4e**, a new peak of F 1s at 685.0 eV was observed in the XPS spectrums of UiO-66-NH_2 after the addition of F^-, which was attributed to that F^- could access to UiO-66-NH_2 for coupling the ligands (Cam Loc Luu 2015). Meanwhile, the binding energy of N1s in UiO-66-NH_2+F^- shifted from 399.6 to 399.9 eV, which was ascribe to formation of hydrogen bond between F^- and amino group (**Fig. 4f**), resulting in the increase of negative charge density

on the N atoms and the decrease of the binding energy of N in amino groups. These resulted demonstrated that the fluorescence enhancement of UiO-66-NH_2 induced by F^- was attributed to the interaction of F^- with free amino groups of NH_2-UiO-66.

3.5 The fluorescent sensor array for the quantification of anions

Based on the above findings, the proposed sensor array can be used to quantify the five anions (F^-, PO_4^{3-}, ClO_4^{4-}, NO_3^-, and SO_4^{2-}). To achieve optimal performance, some parameters in terms of incubation time and probe concentration were assessed. As depicted in **Fig. S6a**, to balance the two signals of UiO-66-NH_2 and UiO-66-OH for anions analysis, the optimized incubation time was determined to be 4 min. Meanwhile, the proposed sensor array could effectively distinguish the five anions when the ratio of UiO-66-NH_2 or UiO-66-OH and anions were 2:1 (**Fig. S6b**). Under the above optimal conditions, we tested the ability of sensor array to distinguish different concentrations of individual anions. Wherein, F^- with different concentration (10-100 μM) were efficiently distinguished by the HCA and LDA (**Fig. 4g and 4h**). Meanwhile, the value of factor 1 in LDA and the concentration of F^- in the range of 10-100 μM presented a good linear correlation(**Fig. 4i**), and the limit of detection (LOD) for F^- was calculated about 2.31 μM based on the 3σ/k (Wei et al. 2023). In addition, quantitative results for other four anions (NO_3^-, ClO_4^-, PO_4^{3-}, and SO_4^{2-}) were obtained in **Fig. S7**, and the calculated LODs were 3.15, 3.21, 2.14, and 3.51 μM, respectively (**Table S3**).

Following, the capacity of the proposed sensor array for the identification of anions mixtures was further studied. The mixtures of ClO_4^- and F^- with varying molar ratios were prepared (ClO_4^-/ F^- = 0:100, 20:80, 50:50, 80:20, and 100:0), which was detected by the sensor array. As shown in **Fig. 4j** and **4k**, LDA results indicated that ClO_4^-/ F^- mixtures at different molar ratios could be identified, and HCA results showed the accurate classification of ClO_4^-/ F^- mixtures into their respective categories. Meanwhile, the ternary mixtures (ClO_4^-, PO_4^{3-}, and SO_4^{2-}) at different molar ratios were further studied, and the results indicated that the proposed sensor array also exhibited good identification capabilities for ternary mixtures of anions **(Fig. 4l** and **S8**). Therefore, these findings demonstrated that a blend comprising various phenolic pollutants could be detected by using the proposed Pt-based nanozyme sensor array. In addition, multiple typical cations (Na^+, K^+, Mg^{2+}, Zn^{2+}, Fe^{2+}, and Ca^{2+}) was introduced into the sensor array as the interfering substance. As shown in **Fig. S9**, all interfering substances were

completely separated from anions, indicating the excellent anti-interference ability. These results proved the good performance of the proposed sensor array for the identification of anions and their mixtures, laying a good foundation for the detection of anions in actual samples.

3.6 Fluorescent sensor array for the detection of real water samples

To evaluate the applications for the identification of multiple anions in real samples, three real water samples (river water, tap water, and lake water) were selected. Wherein, three water samples were spiked into different anions and detected by the proposed sensor array. As shown in **Fig. S10**, five anions and blank groups in river water samples were well separated, and the LDA results showed distinct distributions of blank samples and five phenolic pollutants, with no overlap observed. Similarly, consistent results were obtained in tap water and lake water samples (**Fig. S11** and **S12**), indicating the good distinguishing capacity of the proposed sensor array for anions in tap water samples.

Moreover, the artificial neural network (ANN), an algorithm to imitate the structure and function of a biological neural network, was employed to integrate with the nanozyme sensor array for further assess the actual performance of the proposed sensor array. First, 71.4% and 28.6% of original data set (two LMOFs × five anions and 1 blank group×7 replicates) of river water samples were divided into the training set (n=60) and the testing set (n=24), respectively (**Fig. 5a**), and schematic of ANN algorithm for five anions in river water samples was presented **Fig. 5b**. As shown in **Fig. 5c-f**, the results of ANN algorithm demonstrated that the accuracy of training and test sets were all 100%. Meanwhile, training and test sets obtained from the original data of tap water and lake water samples also achieve good accuracy (**Fig. S13** and **S14**). The above results indicated that machine learning-assisted sensor arrays enabled precise qualitative identification of phenolic pollutants in actual water samples. To further assess the applicability in real samples, machine learning-assisted sensor array was employed to identify 15 blind samples in different water samples, respectively. As shown in **Fig. 5g**, the predicted and true results in river water samples were highly consistent in the confusion matrix, achieving an overall accuracy of 100%, and similar results were obtained with tap water and lake water samples (**Fig. S15**). Meanwhile, the detection results were also provided in **Tables S4-S6**. In conclusion, machine learning-supported nanozyme sensor array based on four Pt nanozymes

enabled the screening of phenolic pollutants in real samples.

4. Conclusion

In conclusion, a machine learning-supported fluorescent sensor array composed of UiO-66-NH_2 and UiO-66-OH was successfully developed for the rapid discrimination of five anions. The proposed sensor array exhibited fluorescence enhancing responses to different anions, generating diverse response patterns for discrimination, which could accurately discriminate individual anions at different concentrations and their mixtures. In addition, the integration of machine learning and fluorescent sensor array enabled the good performance for discriminating anions in real water samples and blind samples, which could carve a promising way to expand the application of sensor arrays for environmental monitoring.

CRediT authorship contribution statement

Dali Wei: Writing-original draft, Data curation, Methodology, Project administration. **Yudi Yang**: Investigation, Software. **Ying Wang**: Software. **Yunxiang Fan**: Data curation, Formal analysis. **Yuxuan Shen**: Data curation, Validation. **Chunmeng Deng**: Software, Validation. **Kun Zeng**: Visualization. **Zhugen Yang**: Conceptualization, Validation. **Zhen Zhang**: Conceptualization, Project administration.

Declaration of competing interest

The authors declare that they have no known competing financial interests or personal relationships that could have appeared to influence the work reported in this paper.

Acknowledgements

This work was supported by the National Natural Science Foundation of China (Grants No. 22176075, 22406068), Natural Science Foundation of Jiangsu Province (BK20240884).

Data availability

Data will be made available on request.

References

Al-Saidi, H.M., Khan, S., 2022. Recent Advances in Thiourea Based Colorimetric and Fluorescent Chemosensors for Detection of Anions and Neutral Analytes: A Review. Crit Rev Anal Chem, 1-17.

Amali, R.K.A., Lim, H.N., Ibrahim, I., Huang, N.M., Zainal, Z., Ahmad, S.A.A., 2021. Significance of nanomaterials in electrochemical sensors for nitrate detection: A review. Trends in Environmental Analytical Chemistry 31.

Cam Loc Luu, T.T.V.N., Tri Nguyen and Tien Cuong Hoang, 2015. Synthesis, characterization and adsorption ability of UiO-66-NH_2. Advances in Natural Sciences: Nanoscience and Nanotechnology 6, 7.

Cao, F., Jaunat, J., Sturchio, N., Cances, B., Morvan, X., Devos, A., Barbin, V., Ollivier, P., 2019. Worldwide occurrence and origin of perchlorate ion in waters: A review. Sci Total Environ 661, 737-749.

Chun-Yi Sun, X.-L.W., * Chao Qin,* Jun-Ling Jin, Zhong-Min Su,* Peng Huang, and Kui-Zhan Shao, 2013. Solvatochromic Behavior of Chiral Mesoporous Metal Organic Frameworks and Their Applications for Sensing Small Molecules and Separating Cationic Dyes. Chem. Eur. J. 19, 6.

Fan, Q., Wang, J., Biazik, J.M., Geng, S., Mazur, F., Li, Y., Ke, P.C., Chandrawati, R., 2023. UiO-66-NH2 Metal–Organic Framework for the Detection of Alzheimer's Biomarker Aβ (1-42). ACS Applied Bio Materials 7(1), 182-192.

Fang, C., Naidu, R., 2023. A review of perchlorate contamination: Analysis and remediation strategies. Chemosphere.

Goshisht, M.K., Tripathi, N., 2021. Fluorescence-based sensors as an emerging tool for anion detection: mechanism, sensory materials and applications. Journal of Materials Chemistry C 9(31), 9820-9850.

Guo, Y., Li, J., Chai, S., Yao, J., 2017. Nanomaterials for the optical detection of fluoride. Nanoscale 9(45), 17667-17680.

Huilin Zhu, J.H., Qingya Zhou, Zhiwei Lv, Cuiyu Li, Gang Hu, 2019. Enhanced luminescence of NH2-UiO-66 for selectively sensing fluoride anion in water medium. Journal of Luminescence 208, 8.

Ihde, M.H., Tropp, J., Diaz, M., Shiller, A.M., Azoulay, J.D., Bonizzoni, M., 2022. A Sensor Array for the Ultrasensitive Discrimination of Heavy Metal Pollutants in Seawater. Advanced Functional Materials 32(33).

Jing, W., Yang, Y., Shi, Q., Wang, Y., Liu, F., 2024. Machine Learning-Based Nanozyme Sensor Array as an Electronic Tongue for the Discrimination of Endogenous Phenolic Compounds in Food. Analytical Chemistry 96(40), 16027-16035.

Kodamatani, H., Kubo, S., Takeuchi, A., Kanzaki, R., Tomiyasu, T., 2023. Sensitive Detection of Nitrite and Nitrate in Seawater by 222 nm UV-Irradiated Photochemical Conversion to Peroxynitrite and Ion Chromatography-Luminol Chemiluminescence System. Environ Sci Technol 57(14), 5924-5933.

Li, M., Pan, Q., Wang, J., Wang, Z., Peng, C., 2024. Machine learning-assisted fluorescence sensor array for qualitative and quantitative analysis of pyrethroid pesticides. Food

Chemistry 433.

Lin, Q., Gong, G.F., Fan, Y.Q., Chen, Y.Y., Wang, J., Guan, X.W., Liu, J., Zhang, Y.M., Yao, H., Wei, T.B., 2019. Anion induced supramolecular polymerization: a novel approach for the ultrasensitive detection and separation of F^-. Chem Commun 55(22), 3247-3250.

Liu, J., Zhan, Y., Qiu, B., Lin, Z., Guo, L., 2023. Portable Smartphone Platform Based on Aggregation-Induced Enhanced Emission Carbon Dots for Ratiometric Quantitative Sensing of Fluoride Ions. ACS Sens 8(2), 884-892.

Liu, Y., Fan, J., Zhang, N., Xu, H., Su, W., Qin, Y., Jiang, D., 2022. Trihexyltetradecylphosphonium chloride based ratiometric fluorescent nanosensors for multiplex anion discrimination. Analyst 147(14), 3209-3218.

Lu, Z., Lu, N., Xiao, Y., Zhang, Y., Tang, Z., Zhang, M., 2022. Metal-Nanoparticle-Supported Nanozyme-Based Colorimetric Sensor Array for Precise Identification of Proteins and Oral Bacteria. ACS Appl Mater Interfaces 14(9), 11156-11166.

Meng, H., Wang, Y., Wu, R., Li, Y., Wei, D., Li, M., Zhu, N., Zhu, F., Zhang, Z., Zhao, H., 2023. Identification of multi-component metal ion mixtures in complex systems using fluorescence sensor arrays. J Hazard Mater 455, 131546.

Moumen, E., Bazzi, L., El Hankari, S., 2022. Metal-organic frameworks and their composites for the adsorption and sensing of phosphate. Coordination Chemistry Reviews 455.

Nawaz, H., Zhang, J., Tian, W., Jin, K., Jia, R., Yang, T., Zhang, J., 2020. Cellulose-based fluorescent sensor for visual and versatile detection of amines and anions. J Hazard Mater 387, 121719.

Norton, A.E., Sharma, M., Cashen, C., Dourges, M.A., Toupance, T., Krause, J.A., Motkuri, R.K., Connick, W.B., Chatterjee, S., 2021. pH-Mediated Colorimetric and Luminescent Sensing of Aqueous Nitrate Anions by a Platinum(II) Luminophore@Mesoporous Silica Composite. ACS Appl Mater Interfaces 13(14), 16197-16209.

Qiaoyin Li, H.C., Shumin You, Zhenyu Lin, Zhitao Chen, Fengping Huang, Bin Qiu, 2023. Colorimetric and fluorescent Dual-Modality sensing platform based on UiO-66 for fluorion detection. Microchemical Journal 186, 6.

Rada, Z.H., Abid, H.R., Shang, J., Sun, H., He, Y., Webley, P., Liu, S., Wang, S., 2016. Functionalized UiO-66 by Single and Binary $(OH)_2$ and NO_2 Groups for Uptake of CO_2 and CH4. Industrial & Engineering Chemistry Research 55(29), 7924-7932.

Ray, B., Sangavi, V., Vishwakarma, S., Parmar, S., Datar, S., 2024. Breath Analysis Using Quartz Tuning Forks for Predicting Blood Glucose Levels Using Artificial Neural Networks. ACS Sensors 9(10), 5468-5478.

Sharifi, H., Tashkhourian, J., Hemmateenejad, B., 2021. An array of metallic nanozymes can discriminate and detect a large number of anions. Sensors and Actuators B: Chemical 339.

Song, D., Zou, Y., Tian, T., Ma, Y., Huang, H., Li, Y., 2024. Machine learning-assisted melamine-Cu nanozyme and cholinesterase integrated array for multi-category pesticide

intelligent recognition. Biosensors and Bioelectronics 266.

Sun, Y., Sun, L., Feng, D., Zhou, H.C., 2016. An In Situ One-Pot Synthetic Approach towards Multivariate Zirconium MOFs. Angew Chem Int Ed Engl 55(22), 6471-6475.

Sun, Z., Fan, Y.Z., Du, S.Z., Yang, Y.Z., Ling, Y., Li, N.B., Luo, H.Q., 2020. Conversion of Fluorescence Signals into Optical Fingerprints Realizing High-Throughput Discrimination of Anionic Sulfonate Surfactants with Similar Structure Based on a Statistical Strategy and Luminescent Metal-Organic Frameworks. Anal Chem 92(10), 7273-7281.

Wang, D., Xin, Y., Li, X., Wang, F., Wang, Y., Zhang, W., Zheng, Y., Yao, D., Yang, Z., Lei, X., 2021. A universal approach to turn UiO-66 into type 1 porous liquids via post-synthetic modification with corona-canopy species for CO_2 capture. Chemical Engineering Journal 416.

Wang, Q.H., Yu, L.J., Liu, Y., Lin, L., Lu, R.G., Zhu, J.P., He, L., Lu, Z.L., 2017. Methods for the detection and determination of nitrite and nitrate: A review. Talanta 165, 709-720.

Wang, X., Qin, L., Zhou, M., Lou, Z., Wei, H., 2018. Nanozyme Sensor Arrays for Detecting Versatile Analytes from Small Molecules to Proteins and Cells. Anal Chem 90(19), 11696-11702.

Wang, X., Wang, X., 2022. UiO-66-NH_2 based fluorescent sensing for detection of tetracyclines in milk. RSC Advances 12(36), 23427-23436.

Wei, D., Li, M., Ai, F., Wang, K., Zhu, N., Wang, Y., Yin, D., Zhang, Z., 2023. Fabrication of Biomimetic Cascade Nanoreactor Based on Covalent Organic Framework Capsule for Biosensing. Analytical Chemistry 95(29), 11052-11060.

Wei, D., Zhang, H., Tao, Y., Wang, K., Wang, Y., Deng, C., Xu, R., Zhu, N., Lu, Y., Zeng, K., Yang, Z., Zhang, Z., 2024. Dual-Emission Single Sensing Element-Assembled Fluorescent Sensor Arrays for the Rapid Discrimination of Multiple Surfactants in Environments. Analytical Chemistry 96(12), 4987-4996.

Wu, M., Yang, B., Shi, L., Tang, Q., Wang, J., Liu, W., Li, B., Jin, Y., 2023. Peroxidase-Mimicking DNAzymes as Receptors for Label-Free Discriminating Heavy Metal Ions by Chemiluminescence Sensor Arrays. Anal Chem 95(6), 3486-3492.

Wu, Z., Yang, H., Pan, S., Liu, H., Hu, X., 2020. Fluorescence-Scattering Dual-Signal Response of Carbon Dots@ZIF-90 for Phosphate Ratiometric Detection. ACS Sens 5(7), 2211-2220.

Xin, Y., Wang, D., Yao, D., Ning, H., Li, X., Ju, X., Zhang, Y., Yang, Z., Xu, Y., Zheng, Y., 2022. Post-synthetic modification of UiO-66-OH toward porous liquids for CO_2 capture. New Journal of Chemistry 46(5), 2189-2197.

Xu, R., Yang, Y., Xu, M., Tao, Y., Deng, C., Li, M., Wei, D., Deng, Y., Lv, J., Wu, C., Zhang, Z., 2024. Screening and discrimination of phenolic acids using bimetallic nanozymes based colorimetric sensor array. Sensors and Actuators B: Chemical 420.

Yaqiong Zhang, L.Z., 2021. Designed multifunctional ratiometric fluorescent probe for directly detecting fluoride ion/ dichromate and indirectly monitoring urea. Journal of Hazardous Materials 418, 11.

Yi, K., Zhang, L., 2020. Embedding dual fluoroprobe in metal-organic frameworks for continuous visual recognition of Pb^{2+} and PO_4^{3-} via fluorescence 'turn-off-on' response: Agar test paper and fingerprint. J Hazard Mater 389, 122141.

Yu, T., Fu, Y., He, J., Zhang, J., Xianyu, Y., 2023. Identification of Antibiotic Resistance in ESKAPE Pathogens through Plasmonic Nanosensors and Machine Learning. ACS Nano 17(5), 4551-4563.

Zhang, C., Li, L., Liu, Q., Chen, Z., 2020. Colorimetric Differentiation of Multiple Oxidizing Anions Based on Two Core-Shell Au@Ag Nanoparticles with Different Morphologies as Array Recognition Elements. Anal Chem 92(10), 7123-7129.

Zhou, C., Xu, W., Zhang, P., Jiang, M., Chen, Y., Kwok, R.T.K., Lee, M.M.S., Shan, G., Qi, R., Zhou, X., Lam, J.W.Y., Wang, S., Tang, B.Z., 2019. Engineering Sensor Arrays Using Aggregation-Induced Emission Luminogens for Pathogen Identification. Advanced Functional Materials 29(4).

Zhou, Y., Zhang, J.F., Yoon, J., 2014. Fluorescence and colorimetric chemosensors for fluoride-ion detection. Chem Rev 114(10), 5511-5571.

Zhu, X., Li, B., Yang, J., Li, Y., Zhao, W., Shi, J., Gu, J., 2014. Effective Adsorption and Enhanced Removal of Organophosphorus Pesticides from Aqueous Solution by Zr-Based MOFs of UiO-67. ACS Applied Materials & Interfaces 7(1), 223-231.

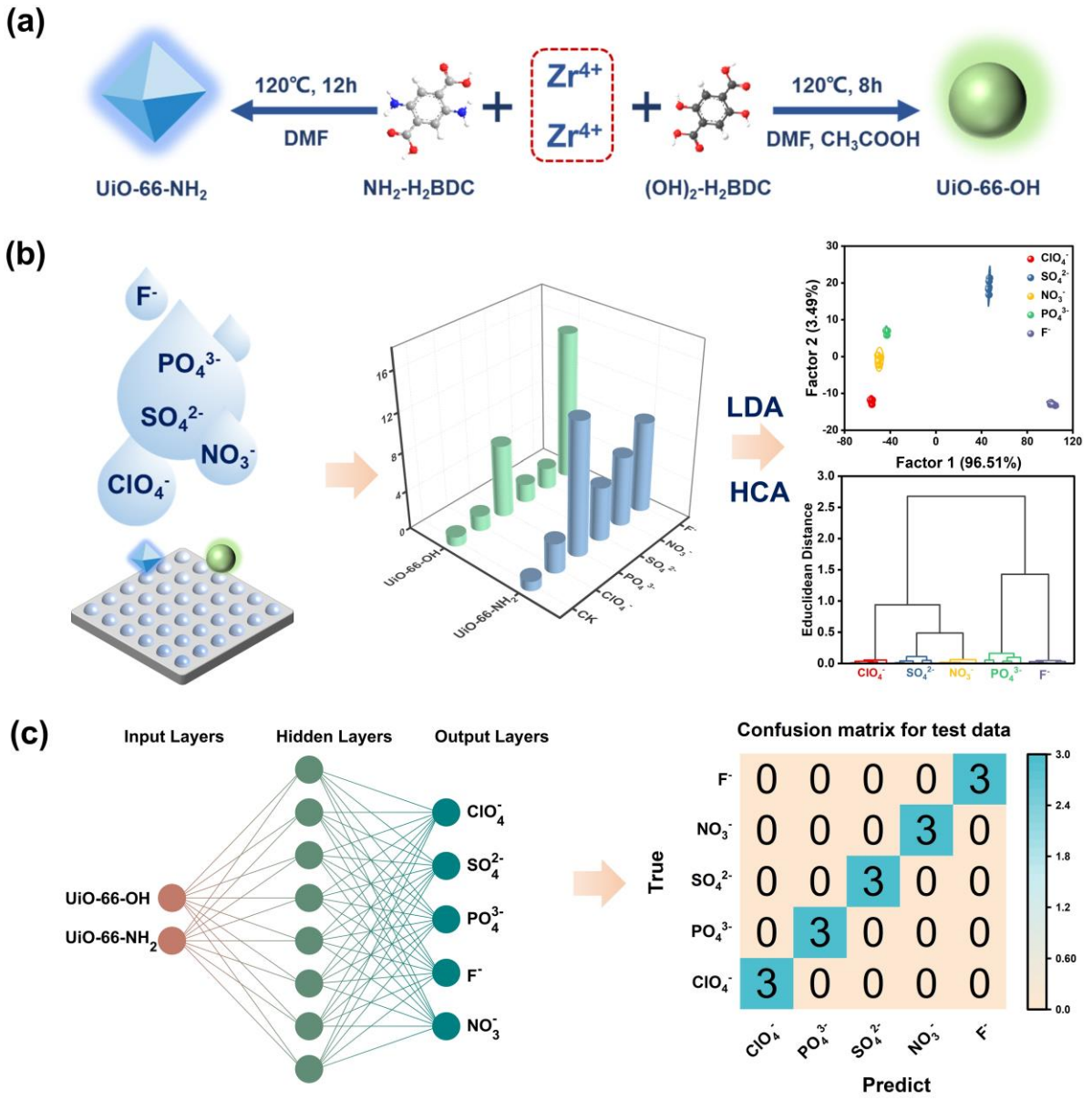

Scheme 1. (a) Schematic diagram of the preparation of UiO-66-NH_2 and UiO-66-OH. (b) The fabrication of the fluorescence sensor array and the application for discrimination of multiple anions. (c) Machine learning-assisted sensor array for identification of anions in actual samples.

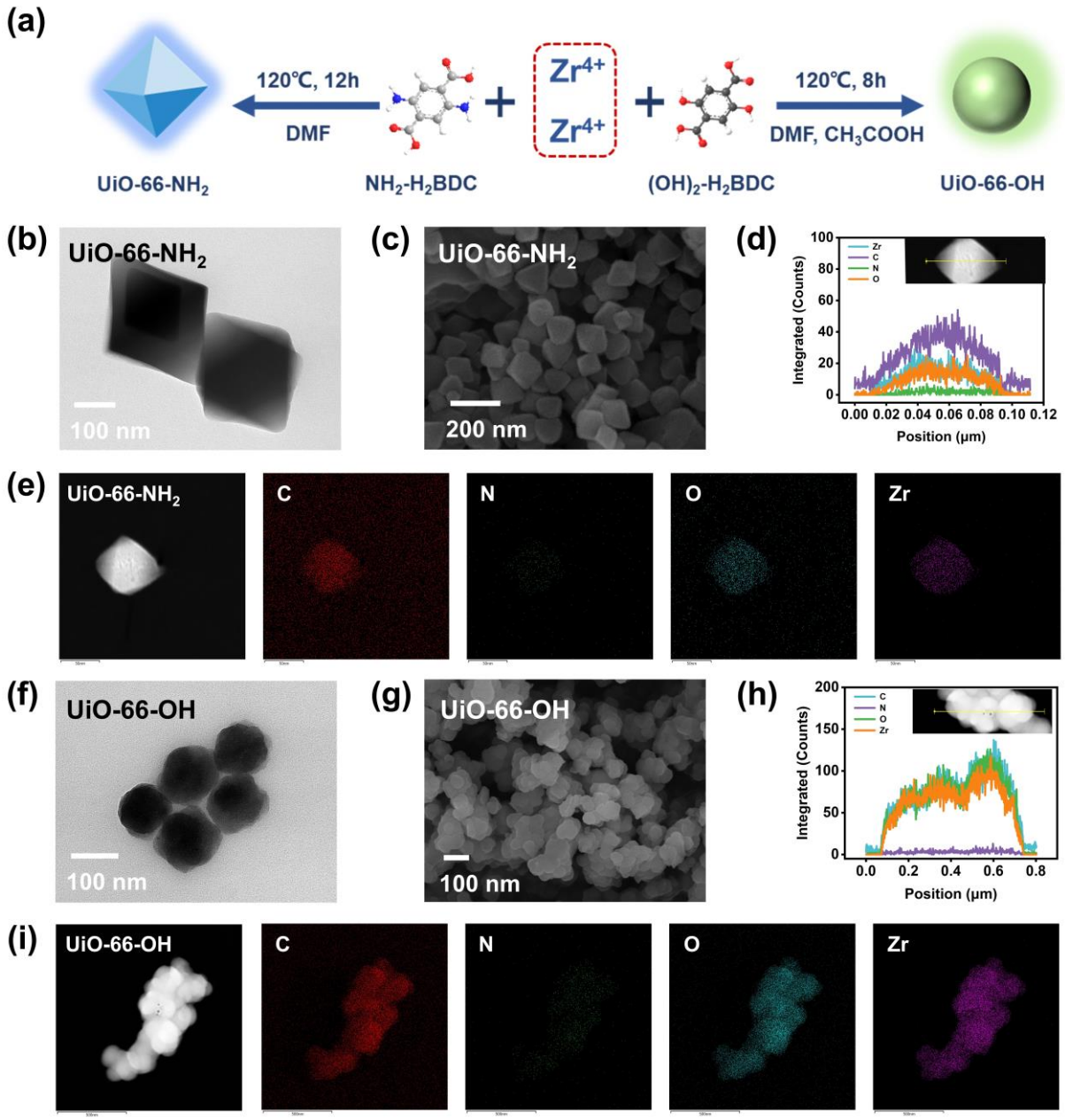

Fig. 1. (a) Schematic diagram of the synthesis of UiO-66-NH_2 and UiO-66-OH. (b) TEM and (c) SEM images of UiO-66-NH_2. HAADF and the corresponding EDS (d) elemental line scan (C, N, O, and Zr) and (d) mapping (C, N, O, and Zr) of UiO-66-NH_2. (f) TEM and (g) SEM images of UiO-66-OH. HAADF and the corresponding EDS (h) elemental line scan (C, N, O, and Zr) and (i) mapping (C, N, O, and Zr) of UiO-66-OH.

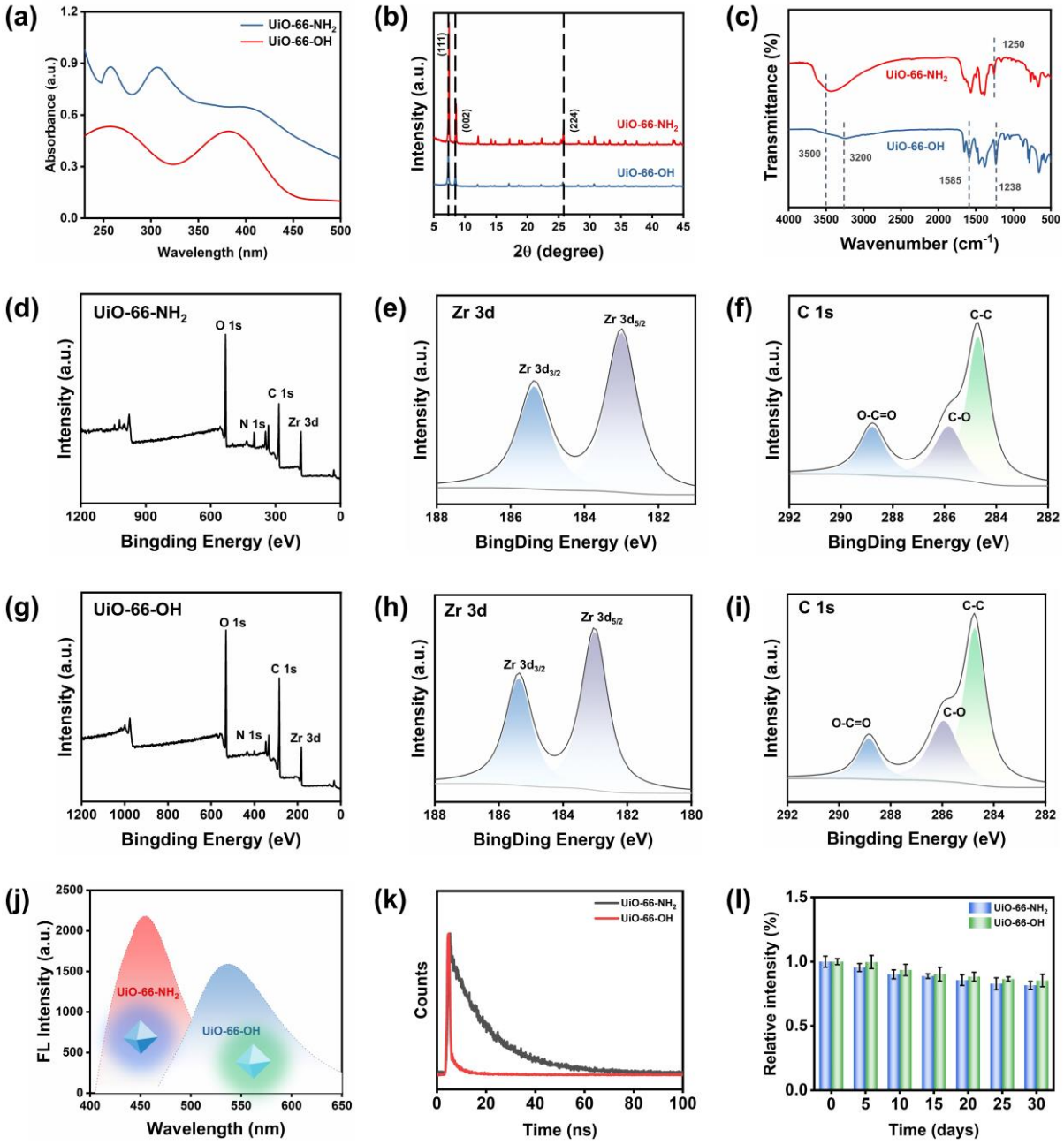

Fig. 2. (a) Ultraviolet absorbance spectra, (b) PXRD patterns, and (c) FT-IR spectra of UiO-66-NH_2 and UiO-66-OH. (d) XPS spectra of UiO-66- NH_2. (e) Zr 3d and (f) C 1s XPS spectra of UiO-66- NH_2. (g) XPS spectra of UiO-66-OH. (h) Zr 3d and C 1s (i) XPS spectra of UiO-66-OH. (j) Fluorescence spectra of UiO-66- NH_2 and UiO-66-OH. (k) Fluorescence lifetime of UiO-66-NH_2 and UiO-66-OH. (l) The stability of two LMOFs under long storage.

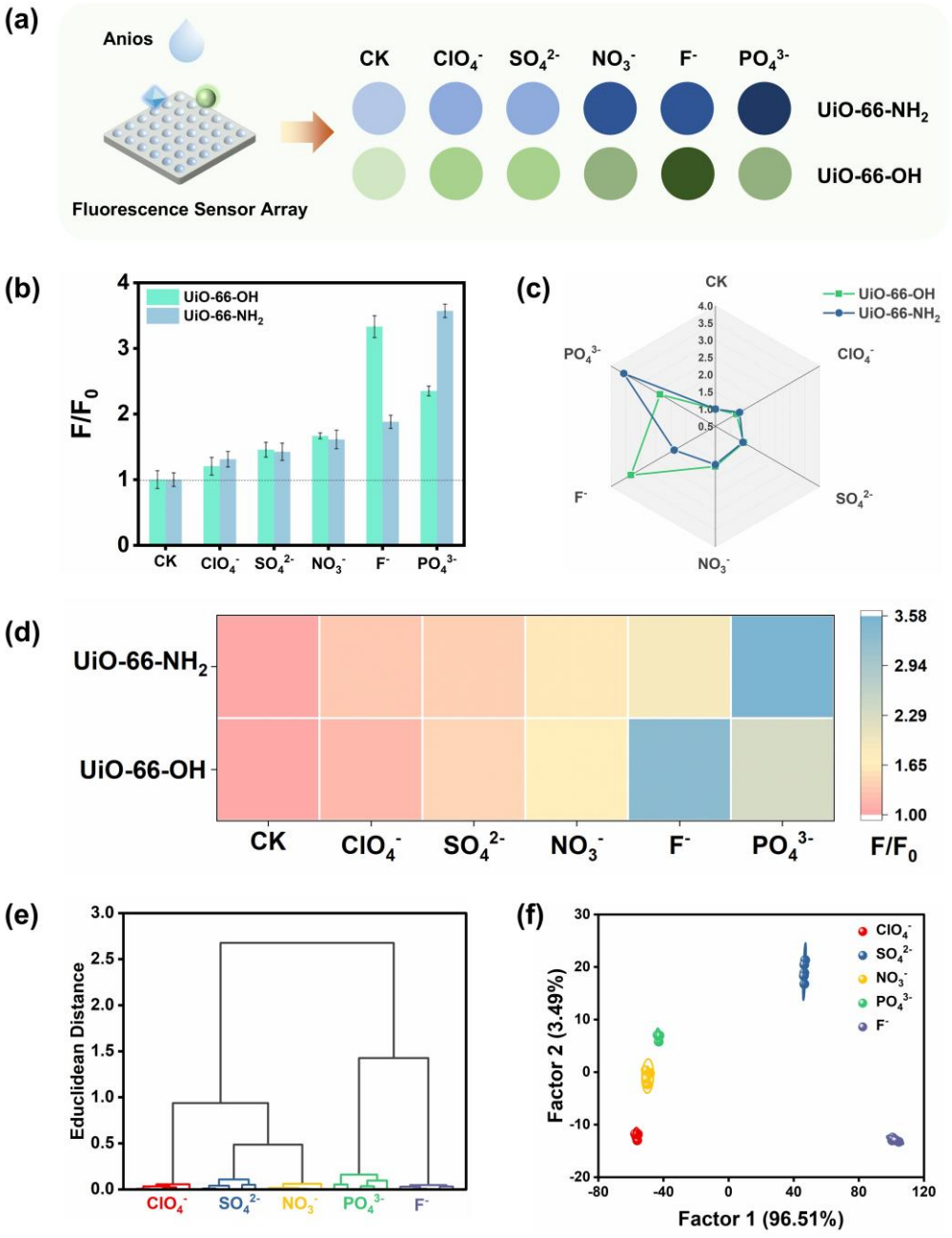

Fig. 3. (a) Schematic diagram showing the fabrication of the fluorescence sensor array based on two LMOFs for anions detection. (b) Fluorescent intensity ratio (F/F_0) responses and (c) Radar plot of UiO-66-NH_2 and UiO-66-OH to five anions (F^-, PO_4^{3-}, ClO_4^-, NO_3^-, and SO_4^{2-}). (d) Two-dimensional heat map generated from fluorescence patterns of fluorescence sensor array. (e) HCA and (f) LDA plot for the identification of five anions derived from the fluorescence-response patterns.

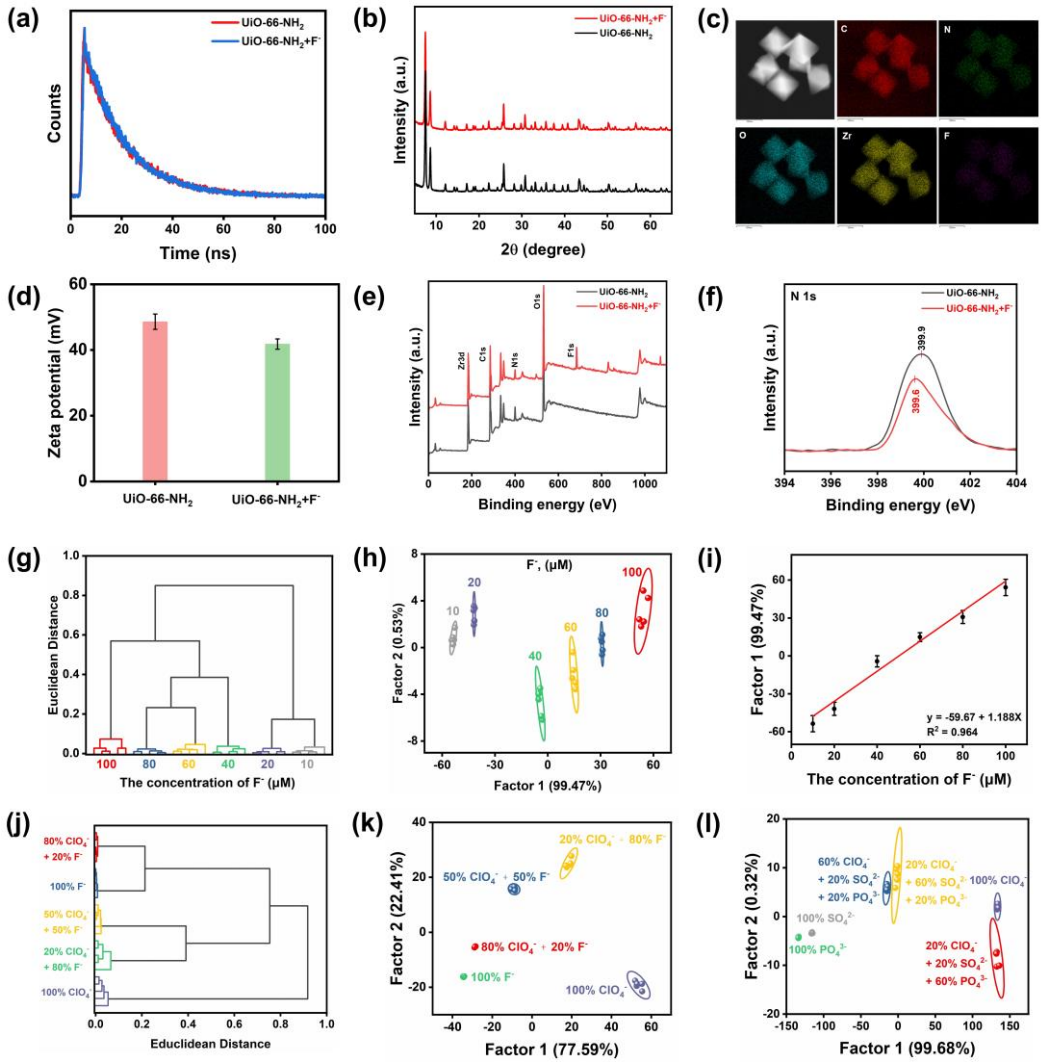

Fig. 4. (a) Fluorescence lifetime of UiO-66-NH_2 and UiO-66-NH_2 in the presence of F^-. (b) XRD patterns of UiO-66-NH_2 before and after treated with F^-. (c) EDS mapping images of UiO-66-NH_2 before and after treated with F^-. (d) Zeta potentials of UiO-66-NH_2 before and after treated with F^-. (e) XPS spectra of UiO-66- NH_2 before and after treated with F^-. (f) XPS spectra of N1s for UiO-66-NH_2 before and after treated with F^-, respectively. (g) HCA and (h) LDA plot for fluorescence response patterns toward different concentrations of F^-. (i) Linear relationships between PC1 and various concentrations of F^-. (j) HCA and (k) LDA plot for fluorescence response patterns toward pure ClO_4^-, pure F^-, and the mixtures of ClO_4^- and F^-. (l) LDA plot for fluorescence response patterns toward pure ClO_4^-, pure SO_4^{2-}, pure PO_4^{3-}, and the mixtures of ClO_4^-, SO_4^{2-}, and PO_4^{3-}.

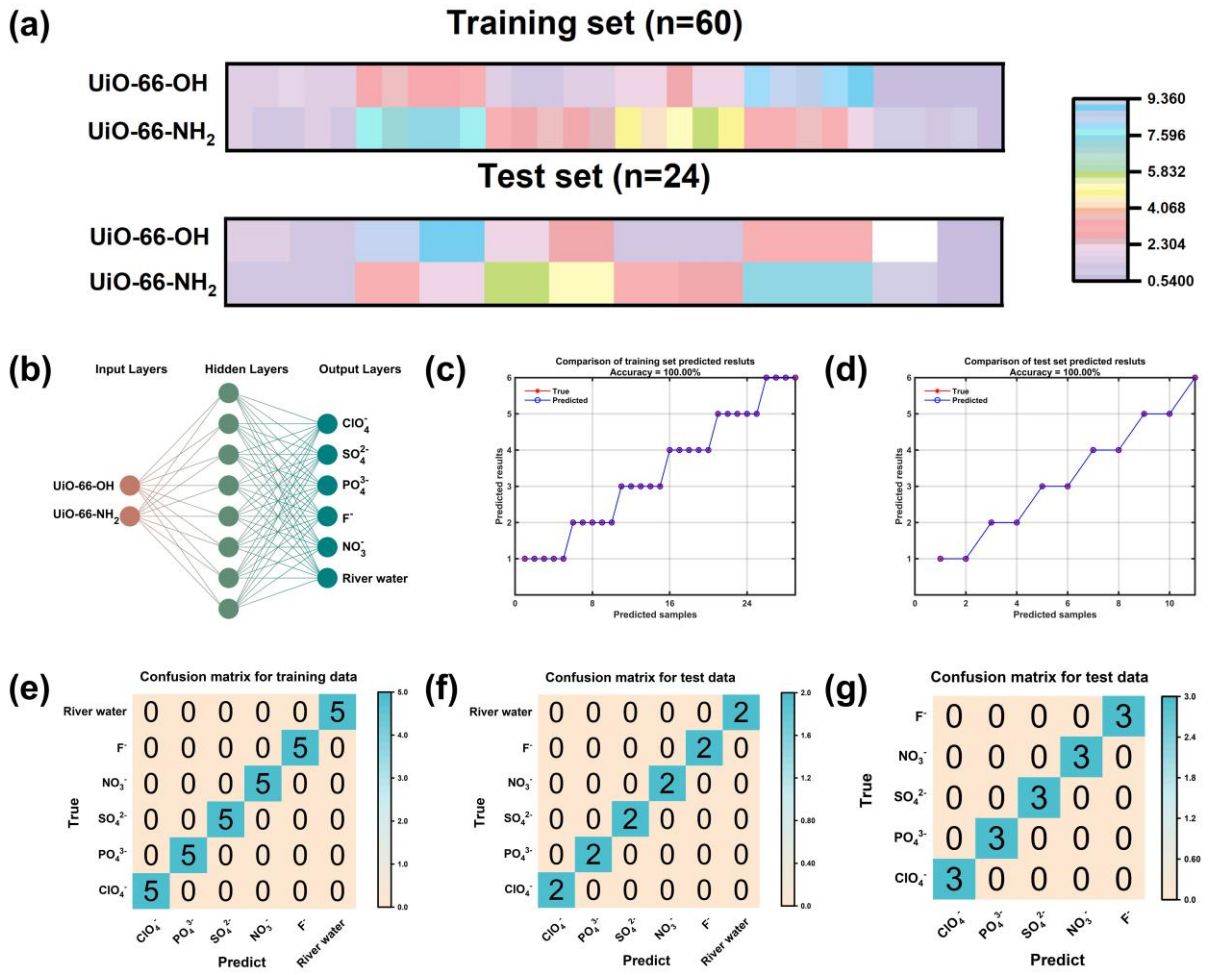

Fig. 5. Machine learning-supported fluorescent sensor array for the identification of five anions in river water samples. (a) Heatmaps of randomly divided training sets (n=60) and test sets (n=24). (b) Schematic of ANN algorithm for five anions in river water samples. Comparison of (c) training set predicted results and (d) test set predicted results. Confusion matrix for (e) training data and (f) test data. (g) Corresponding confusion matrix for five anions in blind river water samples.

Graphic abstract

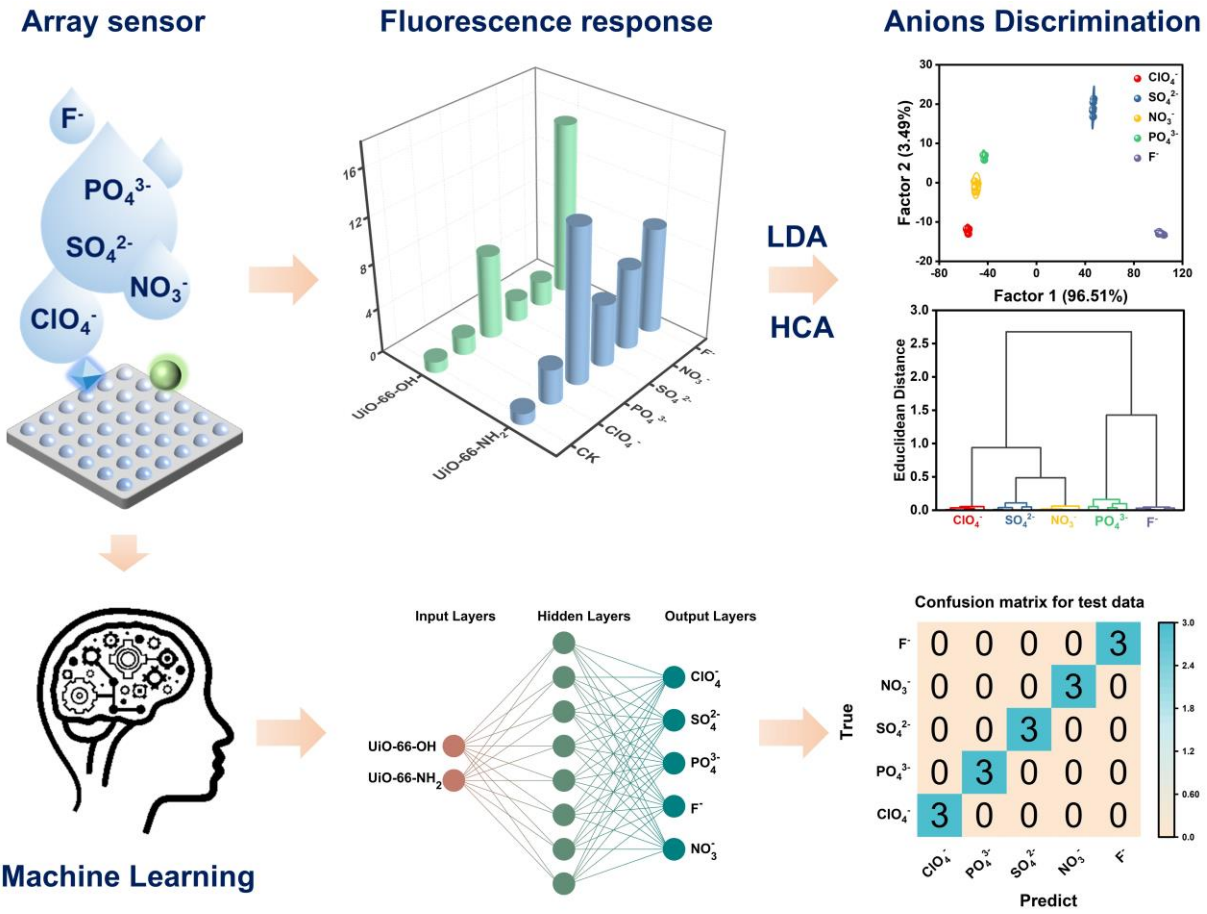

Highlights

(i) Two luminescent metal-organic frameworks were prepared by modifying BDC-NH_2 and BDC-OH on UiO-66.

(ii) A fluorescent sensor array was established for simultaneous discrimination of five anions and their mixtures.

(iii) Assisted by ANN algorithm, fluorescent sensor array achieved accurate identification and prediction of five anions in real water samples.

https://dspace.org/

Machine learning-driven sensor array based on luminescent metal–organic frameworks for simultaneous discrimination of multiple anions

Wei, Dali; Xu, Cheng; Wang, Ying; Feng, Weiwei; Deng, Chunmeng ...

2025-05-15
Elsevier
https://doi.org/10.1016/j.cej.2025.162796
Wei D, Xu C, Wang Y, et al., (2025) Machine learning-driven sensor array based on luminescent metal–organic frameworks for simultaneous discrimination of multiple anions. Chemical Engineering Journal, Volume 512, May 2025, Article number 162796

Downloaded from a DSpace repository. https://dspace.org/